Stress Analysis of Anisotropic Laminated Plates

R. E. ROWLANDS,* T. LIBER,* AND I. M. DANIEL†
IIT Research Institute, Chicago, Ill.
AND
P. G. ROSE‡
Northwestern University, Evanston, Ill.

Membrane and interlaminar stresses in statically loaded and vibrating composite structures are obtained by determining optically and numerically the respective partial derivatives of the holographically recorded transverse displacement field. A clamped, circular, orthotropic boron-epoxy plate under a uniformly applied static pressure and vibration are considered separately. Under uniform static pressure, $\gamma_{r\theta} = 0$, while the anisotropy of the laminated composite results in $\tau_{r\theta} \neq 0$, which is unlike the corresponding isotropic case. The vibrating plate has complicated, unsymmetrical displacements producing both in-plane shearing strains and stresses. The higher order derivatives are obtained optically by holographic-moiré and numerically by employing cubic-spline and discrete-quadratic differentiable functions.

Introduction

MANY structural applications of composites involve transversely loaded plates. While the field equations are well formulated, inherent difficulties aggravate the prospects of obtaining rigorous theoretical analyses to many situations. Based on a previous paper,[1] a completely general experimental method is presented for stress analyzing actual composite plates under static and dynamic conditions. The technique employs a holographically recorded displacement field, from which the stresses and strains (both in-plane and interlaminar) are obtained by differentiation. The method is herein applied to a unidirectionally reinforced, clamped circular boron-epoxy plate. The cases of uniformly applied static pressure and vibration are considered separately. The former is one of the few anisotropic examples for which an analytical solution is available, thereby permitting verification of the experimentally obtained results.

The displacements of the vibrating plate are recorded by time-average holography, while double-exposure holography is used for the static case. Partial derivatives are determined optically from the recorded displacements by holographic-moiré and numerically using piecewise continuous polynomials. Both cubic-spline and discrete-quadratic differentiable functions are employed. The accuracy of these functions for numerically obtaining higher order derivatives has been substantiated previously.[2]

Theory

For laterally loaded plates fabricated from laminated, anisotropic plies which are symmetrically located and oriented about the middle surface, the coupling between bending and stretching vanishes and the governing equations become equivalent to those for a homogeneous plate. If the constitutive equation of the kth ply of the laminate is[3]

$$\{\sigma^k\} = [Q^k]\{\varepsilon^k\} \tag{1}$$

and the strains are expressed in terms of the transverse deflection $w(x, y, t)$ of the middle surface, then the in-plane stresses in the general ply at any time are expressible in terms of this transverse deflection and the stiffness matrix $Q_{ij}{}^k$ of the respective lamina by

$$\begin{Bmatrix} \sigma_x{}^k \\ \sigma_y{}^k \\ \tau_{xy}{}^k \end{Bmatrix} = -z \begin{bmatrix} Q_{11}{}^k & Q_{12}{}^k & 2Q_{16}{}^k \\ Q_{12}{}^k & Q_{22}{}^k & 2Q_{26}{}^k \\ Q_{16}{}^k & Q_{26}{}^k & 2Q_{66}{}^k \end{bmatrix} \begin{Bmatrix} w_{,xx} \\ w_{,yy} \\ w_{,xy} \end{Bmatrix} \tag{2}$$

The interlaminar shear stresses $\tau_{xz}{}^k$, $\tau_{yz}{}^k$ of the kth lamina determined from the equations of motion in the general x- and y-directions are[1]

$$\begin{aligned} \tau_{xz}{}^k &= \sum_{j=1}^{k} \int_{h_{j-1}}^{h_j} z\{Q_{11}{}^j w_{,xxx} + 3Q_{16}{}^j w_{,xxy} + \\ &\quad (Q_{12}{}^j + 2Q_{66}{}^j)w_{,xyy} + Q_{26}{}^j w_{,yyy} - \rho^j w_{,xtt}\}\, dz \\ \tau_{yz}{}^k &= \sum_{j=1}^{k} \int_{h_{j-1}}^{h_j} z\{Q_{16}{}^j w_{,xxx} + (Q_{12}{}^j + 2Q_{66}{}^j)w_{,xxy} + \\ &\quad 3Q_{26}{}^j w_{,xyy} + Q_{22}{}^j w_{,yyy} - \rho^j w_{,ytt}\}\, dz \end{aligned} \tag{3}$$

where t is time, h_j is the distance from the reference surface to the far edge of the jth lamina, and ρ^j is the mass density of the jth ply. Equations (1–3) illustrate that knowing the transverse deflection of the plate as a function of time and position, plus the material properties of the individual plies, membrane and interlaminar stresses can be determined in the plate. In this paper, the displacements are recorded holographically and the derivatives are obtained mechanically and numerically.

Displacement Measurements

Interferometric holography was employed to determine the transverse deflections of the loaded plates. Double exposure holography was used for the statically loaded plate and time-average holography for the vibrating plate. The optical arrangement used to record full-field normal displacement fringes is similar to that of Ref. 1. For double-exposure holography, the out-of-plane displacement w is given by[4]

$$w = [(2N-1)/4]\lambda \tag{4}$$

where N is the holographic fringe order and λ is the wavelength of light. Helium-neon illumination of wavelength $\lambda = 6328$ Å was employed. With time-average holography applied to a sinusoidally vibrating object in which the exposure duration is long compared to the period of the vibration, the amplitude of vibration $w^\circ(x, y)$ is related to the roots of the zero-order Bessel function J_o. That is, a dark fringe is formed whenever

$$J_o[(4\pi/\lambda)w^\circ] = 0, \tag{5}$$

Received July 9, 1973; revision received February 11, 1974. This work is based on a paper presented at the 13th International Congress of Theoretical and Applied Mechanics, Moscow, USSR, August 1972. The authors gratefully acknowledge the assistance of R. R. King, R. LaBedz, and C. W. Nagle of IITRI.

Index categories: Structural Composite Materials; Structural Static Analysis; Structural Dynamic Analysis.

* Senior Research Engineer, Stress Analysis Section.
† Manager, Stress Analysis Section.
‡ Graduate Student.

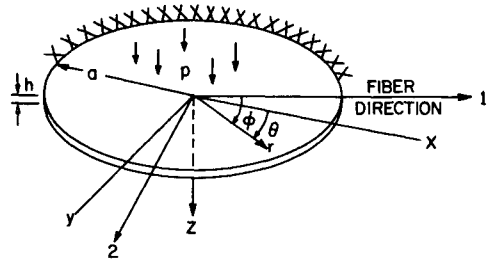

Fig. 1 Schematic diagram of clamped circular plate subjected to transverse loading and coordinate systems.

where

$$w(x, y, t) = w^{\circ} \sin \omega t \tag{6}$$

The frequency of plate vibration is denoted by ω, while the incident and recorded information light beams are both normal to the plate surface. In both cases, the holographic fringes represent loci of material points having constant transverse displacement. Because holographic theory and techniques and applications to static and vibrating isotropic media are amply described in the literature, details of the method are omitted here.

Partial Derivatives

Stresses in normally loaded plates are functions of the spatial and temporal derivatives of the transverse displacements. Second-order derivatives are needed for in-plane stresses, while evaluation of the interlaminar shear stresses requires third-order derivatives, Eqs. (1–3). First-order derivatives of a function ψ can be obtained optically by superposing two transparencies of the fringe pattern representing ψ and displacing one of the transparencies a small amount $\Delta\xi$ relative to the other. The two fringe patterns interfere to generate a moiré pattern representing $\Delta\psi/\Delta\xi$. If the original patterns are sufficiently dense that only small values of $\Delta\xi$ are required, a reasonable approximation to $\partial\psi/\partial\xi$ is obtained. While this concept has been employed in solid mechanics, the method is an approximation over the interval $\Delta\xi$ and boundary definition may be a problem. It presupposes that the original function is optically recorded as contour fringes and furthermore requires this fringe pattern to be dense and of high quality. This optical differentiation technique is basically limited to low-order derivatives.[1,5-9] Speckle-shearing interferometry has very recently also been employed to obtain slopes of surface displacements.[10]

Because of limitations associated with the preceding optical differentiation method, two numerical differentiation techniques are utilized.[2] In both cases, the plate displacements are represented over the interval of interest $[x_o, x_n]$ by piecewise continuous and differentiable functions. The first approach uses the spline concept. The displacement field is fitted by a cubic function in each subinterval defined by the experimental data points. A total of $(4n-2)$ boundary conditions are obtained by passing the cubic polynomials through the $(n+1)$ discrete data points, plus forcing the functions and their first two derivatives to be continuous at the internal mesh points. A cubic polynomial representation of the displacement field is thereby obtained which is continuous and has continuous first and second derivatives throughout the total interval. The function can be readily differentiated analytically at any point within this interval of interest. Reinsch extended the spline concept to provide smooth fits of the cubic polynomial around the discrete data points rather than strict collocation.[11] One noteworthy observation of Reinsch's formulation is that the second derivatives at the end points are taken equal to zero identically as the supplementary boundary conditions. The smoothed spline involves two smoothing parameters: δ and S. Reinsch suggests that S be taken equal to $(n+1)$. δ is an individual data point smoothing parameter and is an estimate of the confidence one has in the data.

An alternate approach to representing the entire interval of interest by essentially one continuous function is to employ a sequence of discrete overlapping quadratic polynomials. The derivatives at the internal mesh point of each subinterval are obtained by analytically differentiating the respective polynomial. The derivatives at the end points are obtained by evaluating the derivatives of the first and last discrete polynomial at these locations, respectively.

Stress Analysis of Plates

Statically Loaded Plate

The displacement fringe pattern for a clamped, circular orthotropic plate subjected to uniform pressure (Fig. 1) was obtained using double-exposure holography and is illustrated in Fig. 2. The plate is a seven-ply unidirectional boron-epoxy laminate of radius $a = 1.625$ in. and thickness $h = 0.038$ in. The boron fibers are horizontal and the uniform pressure p was 0.25 psi. Actual normal plate displacements are obtained from this fringe pattern with the aid of Eq. (4). For this case in which the transverse displacement field is axisymmetrical (Fig. 2), the membrane stresses are related in polar coordinates to the derivatives of the displacement field $w(r)$ by (see Appendix)§

$$\begin{Bmatrix} \sigma_r \\ \sigma_\theta \\ \tau_{r\theta} \end{Bmatrix} = -z \begin{bmatrix} \bar{Q}_{11} & \bar{Q}_{12} & 2\bar{Q}_{16} \\ \bar{Q}_{12} & \bar{Q}_{22} & 2\bar{Q}_{26} \\ \bar{Q}_{16} & \bar{Q}_{26} & 2\bar{Q}_{66} \end{bmatrix} \begin{Bmatrix} \dfrac{d^2w}{dr^2} \\ \dfrac{1}{r}\dfrac{dw}{dr} \\ 0 \end{Bmatrix} \tag{7}$$

while the interlaminar shearing stresses are expressed by (see Appendix):

$$\begin{Bmatrix} \tau_{rz} \\ \tau_{\theta z} \end{Bmatrix} = 1/2\left(z^2 - \frac{h^2}{4}\right) \begin{bmatrix} \bar{Q}_{11} & (\bar{Q}_{12} + 2\bar{Q}_{66}) \\ \bar{Q}_{16} & 3\bar{Q}_{26} \end{bmatrix} \begin{Bmatrix} \dfrac{d^3w}{dr^3} \\ \dfrac{1}{r}\dfrac{d^2w}{dr^2} - \dfrac{1}{r^2}\dfrac{dw}{dr} \end{Bmatrix} \tag{8}$$

For an orthotropic medium, coefficients of the stiffness matrix $\bar{Q}$ relative to the polar coordinate system are related to those in terms of the principal material axes Q by[3]

$$\begin{aligned}
\bar{Q}_{11} &= Q_{11}m^4 + 2(Q_{12} + 2Q_{66})m^2n^2 + Q_{22}n^4 \\
\bar{Q}_{22} &= Q_{11}n^4 + 2(Q_{12} + 2Q_{66})m^2n^2 + Q_{22}m^4 \\
\bar{Q}_{12} &= (Q_{11} + Q_{22} - 4Q_{66})m^2n^2 + Q_{12}(m^4 + n^4) \\
\bar{Q}_{66} &= (Q_{11} + Q_{22} - 2Q_{12} - 2Q_{66})m^2n^2 + Q_{66}(m^4 + n^4) \\
\bar{Q}_{16} &= (Q_{11} - Q_{12} - 2Q_{66})nm^3 + (Q_{12} - Q_{22} + 2Q_{66})n^3m \\
\bar{Q}_{26} &= (Q_{11} - Q_{12} - 2Q_{66})n^3m + (Q_{12} - Q_{22} + 2Q_{66})nm^3
\end{aligned} \tag{9}$$

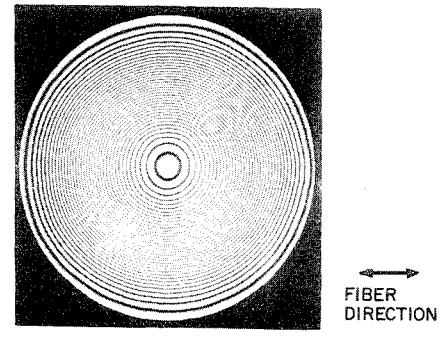

Fig. 2 Holographic fringe pattern of transverse deflection of a clamped circular unidirectional boron-epoxy plate subjected to uniform pressure.

§ It is noteworthy that while the transverse displacement field for a clamped, circular orthotropic plate under uniform pressure is axisymmetrical, that for the same plate subjected to a central load is not, Fig. 3 of Ref. 1.

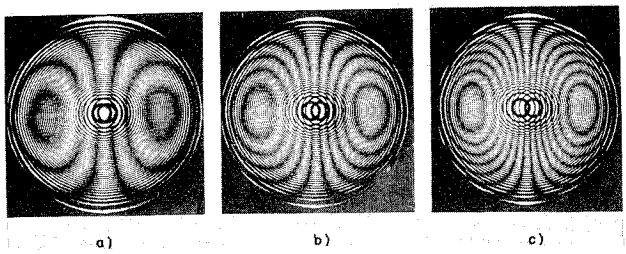

Fig. 3 Loci of constant dw/dr for a clamped circular unidirectional boron-epoxy plate subjected to uniform pressure: a) $\Delta r = 0.099$ in.; b) $\Delta r = 0.155$ in.; c) $\Delta r = 0.22$ in.

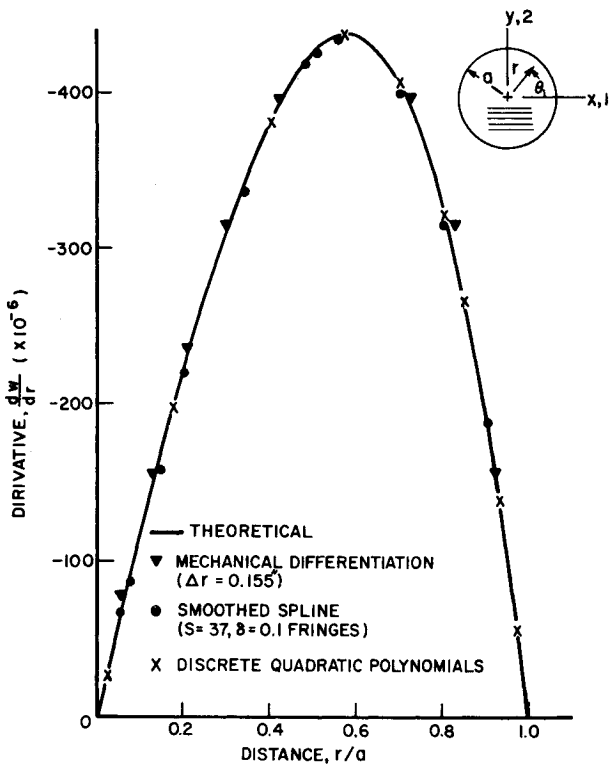

Fig. 4 First-order derivatives for clamped circular unidirectional boron-epoxy plate subjected to uniform pressure.

where $m = \cos\phi$, $n = \sin\phi$, and ϕ is the polar angle measured from the horizontal axis of material symmetry (fiber direction, Fig. 1). The coefficients of the stiffness matrix Q of Eq. (9) are, in turn, related to the four independent engineering constants through the following expressions:

$$\begin{aligned} Q_{11} &= E_{11}/(1-\nu_{12}\nu_{21}) \\ Q_{22} &= E_{22}/(1-\nu_{12}\nu_{21}) \\ Q_{12} &= (\nu_{21}E_{11})/(1-\nu_{12}\nu_{21}) \\ Q_{66} &= G_{12} \end{aligned} \tag{10}$$

where $\nu_{12}E_{22} = \nu_{21}E_{11}$. The orthotropic axes of material symmetry are denoted by 1 and 2, Fig. 1. For the unidirectional boron-epoxy plate employed

$$\begin{aligned} E_{11} &= 30\times10^6 \text{ psi} \\ E_{22} &= 3.0\times10^6 \text{ psi} \\ G_{12} &= 1\times10^6 \text{ psi} \\ \nu_{12} &= 0.3 \end{aligned} \tag{11}$$

For comparison, the first-order derivatives are obtained optically (Fig. 3) and numerically. Sample results are plotted in Fig. 4, as is the theoretical derivative. The fringe patterns representing dw/dr obtained optically by superposing two transparencies of Fig. 2 and translating one transparency $\Delta r = 0.099$ in., 0.155 in., and 0.22 in., respectively, are illustrated in Fig. 3. For simplicity, only the values associated with $\Delta r = 0.155$ are plotted in Fig. 4. The smoothed cubic spline results of Fig. 4 were computed for $S = (n+1) = 37$ (the number of fringes or data points) and $\delta = 0.1$ fringe.

The best smooth curve was drawn through the various first derivatives obtained optically and numerically. By representing these data by discrete quadratic polynomials, differentiating and repeating the process, derivatives up through the third order were obtained. From these displacement derivatives of the transversely loaded plate associated with Fig. 2, Eqs. (7–10), and the material properties of Eq. (11), the membrane and interlaminar stresses were computed and are plotted in Figs. 5–7. The in-plane stresses along the axes of material symmetry ($\tau_{r\theta} = 0$) are plotted in Fig. 5, while those for $\emptyset = \theta = 45°$ are illustrated in Fig. 6. The interlaminar shearing stresses (between plies 3 and 4) are shown in Fig. 7.

The theoretical results are also plotted for comparison in Figs. 5–7. For a homogeneous orthotropic clamped circular plate referred to the principal elastic axes and subjected to uniform lateral pressure p, the transverse deflection w is analytically expressed as[12]

$$w = \frac{pa^4}{64D'}\left(1-\frac{r^2}{a^2}\right) \tag{12}$$

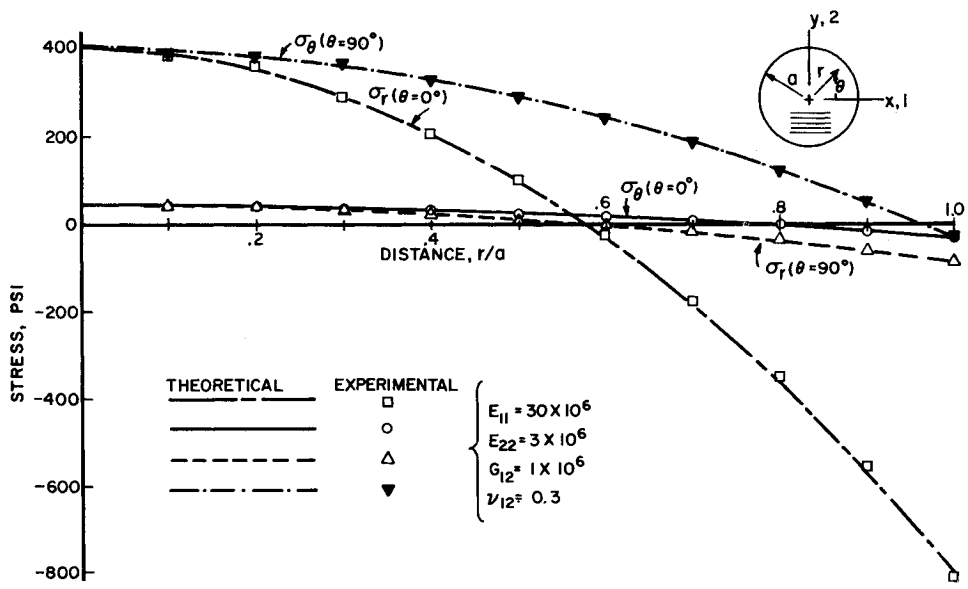

Fig. 5 Stresses along principal material axes in a clamped circular unidirectional boron-epoxy plate subjected to uniform pressure.

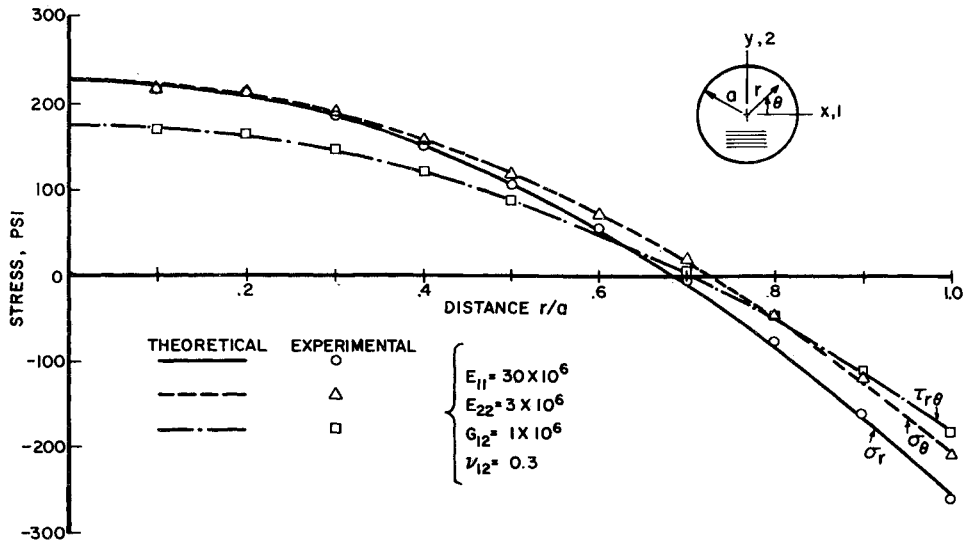

Fig. 6 In-plane stresses along the 45° radius in a clamped circular unidirectional boron-epoxy plate subjected to uniform pressure.

where

$$D' = \tfrac{1}{8}(3D_1+2D_3+3D_2)$$
$$D_1 = h^3Q_{11}/12$$
$$D_2 = h^3Q_{22}/12 \qquad (13)$$
$$D_3 = \nu_{21}D_1+Q_{66}h^3/6$$

For this particular geometry and loading, the transverse displacement field is therefore axisymmetrical, irrespective of whether the mechanical response is orthotropic or isotropic. For isotropy

$$D_1 = D_2 = D_3 = D' = Eh^3/12(1-\nu^2) \qquad (14)$$

The axisymmetric strain field, together with the directional dependent plate properties, results in maximum membrane stresses occurring along the directions of material symmetry, Figs. 5 and 6. While the interlaminar stresses (Fig. 7) are small compared to the in-plane stresses, interply strength depends on the matrix material or laminate adhesive. The latter is typically much weaker than are the fiber-reinforced plies.

Vibrating Plate

Figure 8 is a time-average hologram of basically the same clamped unidirectional boron-epoxy plate which is now sinusoidally vibrated at 2300 Hz. The fibers are again horizontal. The plate was excited from behind by a horn driven by an oscillator-amplifier system. While the deflection field for the clamped circular plate under uniform static pressure is axisymmetrical for both isotropic and anisotropic plates, the directionality of material properties now produces a significantly different deflection pattern during vibration from that of the corresponding isotropic pattern.[1,13]

From the fringe pattern of Fig. 8 and Eqs. (5) and (6), the derivatives $w_{,xx}$, $w_{,xy}$, and $w_{,yy}$ were numerically evaluated (by discrete quadratic representation) along the line A-B. With these derivatives, Eq. (2), and the material properties of Eq. (11), the membrane stresses were obtained along line A-B of Fig. 8 and are plotted in Fig. 9. It should be noted that although $Q_{16} = Q_{26} = 0$ in the principal material directions, all three components of the curvature vector are, in general, nonzero and hence τ_{xy} is not identically zero along A-B. This is unlike the previously considered uniform static loading where $\gamma_{r\theta} = 0$, causing the membrane shear stresses to be identically zero along the axes of material symmetry. The high normal stresses of Fig. 9 in the vicinity of $y = 0.2$ are associated with the trough in the deformed plate at that location.

In spite of extreme attempts to excite the plate of Fig. 8 uniformly, the bottom half of the plate displays a larger maximum deflection than does the top. This lack of symmetry, which likely is at least partly associated with variations in material properties, demonstrates the desire to develop techniques for stress analyzing actual situations.

Since the time-average hologram of Fig. 8 actually records the maximum amplitude of the vibration ($\omega t = \pi/2$), the stresses of Fig. 9 are maximum values. The stresses vary sinusoidally

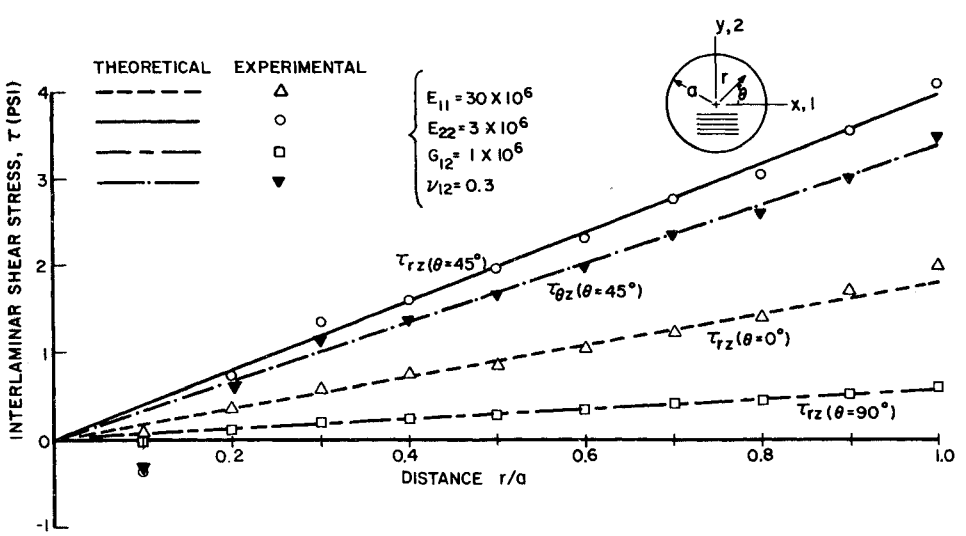

Fig. 7 Interlaminar shear stresses in a clamped circular unidirectional boron-epoxy plate subjected to uniform pressure.

according to Eq. (6) between the positive and negative values of the magnitudes displayed in Fig. 9. However, it is these maximum stresses that are significant in design.

While not done so here, first partial derivatives of the deflection of vibrating plates can also be obtained optically by superposing two transparencies of the holographically (time-average) recorded displacements.[1] Furthermore, by determining the respective third-order partial derivatives, the interlaminar shear stresses could be evaluated for the vibrating plate using Eq. (3). The temporal derivatives of Eq. (3) are then obtainable by analytically differentiating Eq. (6), where the fringes of Fig. 8 represent $w^{\circ}(x, y)$.

Discussion and Conclusions

A method is presented for stress analyzing statically or dynamically loaded laminates. Classical plate theory is assumed in that the membrane and interlaminar stresses are functions of the derivatives of the transverse displacements. The technique is reliable, simple, and expedient, and is applicable to a wide range of problems. It employs experimentally determined displacements, the derivatives of which are obtained optically and numerically. Numerical differentiation is accomplished by representing the measured displacements by piecewise continuous functions which are then differentiated analytically. Both cubic-spline and discrete quadratic differentiable functions are employed, the accuracy of these functions for numerically obtaining higher order derivatives having been substantiated previously by the authors. The general method is employed to stress analyze a unidirectionally reinforced clamped circular boron-epoxy plate. Uniform pressure loading and vibration of the plate are considered separately. The transverse displacement fields were recorded by double-exposure and time-average holography, respectively. The static problem has been solved theoretically and the results serve as a check on the present method. The authors are unaware of other solutions for the vibrating anisotropic laminate.

Like the corresponding isotropic problem, the transverse displacements are axisymmetrical for the statically loaded clamped circular plate. While this polar symmetry causes the strains and curvature to be functions of the radial coordinate only, resulting in $\gamma_{r\theta} = 0$, the anisotropy of the medium makes $\tau_{r\theta} \neq 0$ except along the axes of material symmetry. This is unlike the isotropic case where $\tau_{r\theta} = 0$ throughout. The displacement patterns of the vibrated plate are significantly more complicated. The in-plane shearing stresses and strains are now in general both nonzero. The experimental results agree very well with theory, where the latter is available.

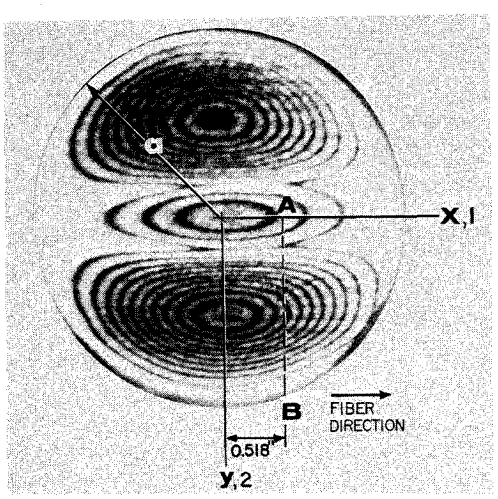

Fig. 8 Holographic fringe pattern of out-of-plane displacements of vibrating boron-epoxy plate (a = 1.61 in.; 2300 Hz).

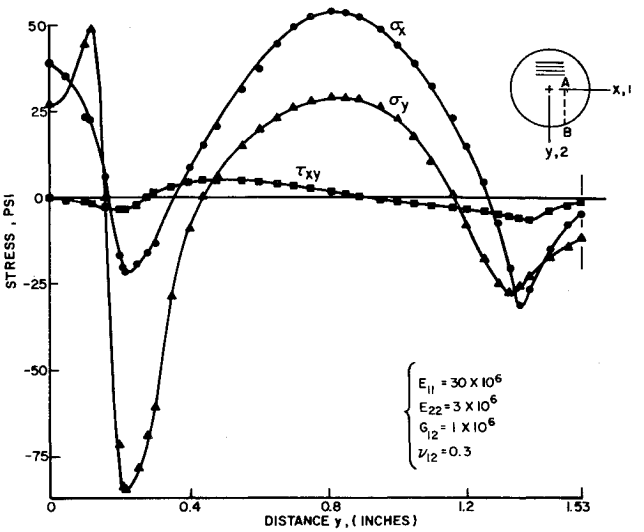

Fig. 9 Stresses along line A-B of vibrating boron-epoxy plate (2300 Hz).

The presented general method of stress analyzing plates is highly compatible with techniques currently being developed for full-field holographic recording of large structural systems under actual operating conditions. It does not necessitate reflective surfaces, is independent of anisotropy and heterogeneity, and is applicable under static or dynamic loading. Of equal technical significance is that the interlaminar shearing stresses in composites can be determined, something not readily attainable by other experimental techniques. The interlaminar shearing stresses produce delamination and interply fracture, this being a cause of catastrophic failure in composite structures. A deficiency in determining displacements holographically is that low fringe densities sometimes occur in regions of greatest interest, i.e., locations of maximum curvature such as at the center and boundary of the statically loaded plate considered here. The sparse fringe density affects the accuracy of the analysis.

Interlaminar shearing stress analysis of dynamically loaded plates requires time derivatives of the displacement field. For sinusoidal vibration as considered here, the time dependency of $w(x, y, t)$ is analytically defined and temporal differentiation is consequently trivial. Time differentiation under transient conditions is more involved. A sequence of displacement fringe patterns must be first recorded at short time intervals, from which temporal derivatives can be determined by either of the herein described differentiation techniques.

Classical theory as employed herein gives rise to one differential equation involving the transverse deflection function w. Stresses, strains, and moments depend only on this function and material properties. For highly anisotropic composites having a width-to-thickness ratio of less than ten, transverse shear can render the Kirchhoff assumption inaccurate.[14,15] While a unique lamination theory including transverse shear has not yet evolved, at least one representation involves two additional unknown functions, ϕ_x and ϕ_y. The stresses, strains, moments, and forces now depend on w, ϕ_x, and ϕ_y. These three functions are analytically defined by three coupled partial differential equations and the boundary conditions, although Ambartsumyan[14] has expressed the response in terms of one sixth-order differential equation. Concomitant with the difficulties in analytically solving simultaneously for w, ϕ_x, and ϕ_y, only the lateral deflection function appears capable of being readily evaluated experimentally. However, laminate width-to-thickness ratios are typically sufficiently large in practice that stresses evaluated using the classical assumptions are normally adequate for engineering purposes and design. In the examples cited here, the width-to-thickness ratio of 80 well justifies neglecting the transverse shear.

The numerical differentiation techniques as presently constituted are basically developed for one independent variable only. This is cumbersome when stress analyzing situations in which the displacement field depends on both x and y, such as the vibrating laminate considered. For expedient analysis of such problems, general extension of the differentiation methods to two or more independent variables merits attention.

The employed stress analysis technique is similar to the currently popular finite-element method in that strains and stresses are evaluated by differentiating an assumed analytical representation, over some region, of the displacement field. The actual displacement field is herein measured, whereas with the finite-element concept it is generated from the stiffness matrix of the structure and applied loads. Displacement-field determination by the latter necessitates knowing or reliably assuming the material constitutive behavior and boundary conditions. This can be difficult with actual components exhibiting nonlinear or inelastic response and subjected to realistic loadings. The price paid for actual rather than mathematically generated displacements is that a physical, rather than mathematical, model must be employed.

Appendix

For a static uniformly loaded circular plate clamped along its boundary, the transverse displacement field is axisymmetrical, be the plate isotropic or orthotropic [Eq. (12), and Refs. 2 and 12], i.e., $w = w(r)$. Using polar coordinates r and θ, the Cartesian differential operators are related to the polar variables by

$$\frac{\partial}{\partial x} = \cos\theta\frac{\partial}{\partial r} - \frac{\sin\theta}{r}\frac{\partial}{\partial\theta} \quad \text{and} \quad \frac{\partial}{\partial y} = \sin\theta\frac{\partial}{\partial r} + \frac{\cos\theta}{r}\frac{\partial}{\partial\theta} \tag{A1}$$

Now as $\theta \to 0$; $\sin\theta \to 0$, $\cos\theta \to 1$, $\sigma_x \to \sigma_r$, $\sigma_y = \sigma_\theta$, $\tau_{xy} \to \tau_{r\theta}$, $\tau_{xz} \to \tau_{rz}$, $\tau_{yz} \to \tau_{\theta z}$, and $Q_{ij} \to \bar{Q}_{ij}$ where the bar denotes with respect to the polar coordinates. From the differential operators of Eq. (A1), and noting that $\partial w/\partial\theta = 0$, the partial spatial derivatives of Eqs. (2) and (3) for this special case become

$$\begin{aligned}
\left.\frac{\partial^2 w}{\partial x^2}\right|_{\substack{\theta=0\\ w,\theta=0}} &= \frac{d^2w}{dr^2} & \left.\frac{\partial^3 w}{\partial x^3}\right|_{\substack{\theta=0\\ w,\theta=0}} &= \frac{d^3w}{dr^3}\\
\left.\frac{\partial^2 w}{\partial y^2}\right|_{\substack{\theta=0\\ w,\theta=0}} &= \frac{1}{r}\frac{dw}{dr} & \left.\frac{\partial^3 w}{\partial x^2\,\partial y}\right|_{\substack{\theta=0\\ w,\theta=0}} &= 0\\
\left.\frac{\partial^2 w}{\partial x\,\partial y}\right|_{\substack{\theta=0\\ w,\theta=0}} &= 0 & \left.\frac{\partial^3 w}{\partial y^3}\right|_{\substack{\theta=0\\ w,\theta=0}} &= 0\\
\left.\frac{\partial^3 w}{\partial x\,\partial y^2}\right|_{\substack{\theta=0\\ w,\theta=0}} &= \frac{1}{r}\frac{d^2w}{dr^2} - \frac{1}{r^2}\frac{dw}{dr}
\end{aligned} \tag{A2}$$

From Eqs. (2) and (A2), the in-plane stresses for the axisymmetrical case are expressed by

$$\begin{Bmatrix} \sigma_r^k \\ \sigma_\theta^k \\ \tau_{r\theta}^k \end{Bmatrix} = -z \begin{bmatrix} \bar{Q}_{11}^k & \bar{Q}_{12}^k & 2\bar{Q}_{16}^k \\ \bar{Q}_{12}^k & \bar{Q}_{22}^k & 2\bar{Q}_{26}^k \\ \bar{Q}_{16}^k & \bar{Q}_{26}^k & 2\bar{Q}_{66}^k \end{bmatrix} \begin{Bmatrix} \dfrac{d^2w}{dr^2} \\ \dfrac{1}{r}\dfrac{dw}{dr} \\ 0 \end{Bmatrix} \tag{A3}$$

Similarly, from Eqs. (3) and (A2), the interlaminar shearing stresses between the h_j and h_{j+1} laminae are

$$\begin{aligned}
\tau_{rz}^k &= \sum_{j=1}^{k} \int_{h_{j-1}}^{h_j} z\left\{\bar{Q}_{11}^j\frac{d^3w}{dr^3} + (\bar{Q}_{12}^j + 2\bar{Q}_{66}^j)\left(\frac{1}{r}\frac{d^2w}{dr^2} - \frac{1}{r^2}\right)\frac{dw}{dr}\right\}dz\\
\tau_{\theta z}^k &= \sum_{j=1}^{k} \int_{h_{j-1}}^{h_j} z\left\{\bar{Q}_{16}^j\frac{d^3w}{dr^3} + 3\bar{Q}_{26}^j\left(\frac{1}{r}\frac{d^2w}{dr^2} - \frac{1}{r^2}\frac{dw}{dr}\right)\right\}dz
\end{aligned} \tag{A4}$$

For a unidirectional plate of total thickness h, Eqs. (A4) simplify to Eqs. (8) for the shear stress at the distance z from the neutral surface.

References

[1] Rowlands, R. E. and Daniel, I. M., "Application of Holography to Anisotropic Composite Plates," *Experimental Mechanics*, Vol. 12, No. 2, Feb. 1972, pp. 75–82.

[2] Rowlands, R. E., Liber, T., Daniel, I. M., and Rose, P. G., "Higher-Order Numerical Differentiation of Experimental Information," *Experimental Mechanics*, Vol. 13, No. 3, March 1973, pp. 105–112.

[3] Arvin, G. H., ed., "Structural Design Guide for Advanced Composite Applications," AFML F33615-69-C-1368, Aug. 1969, North American Rockwell Corp., Los Angeles, Calif.

[4] Collier, R. J., Burckhardt, C. B., and Lin, L. H., *Optical Holography*, Academic Press, New York, 1971.

[5] Theocaris, P. S., *Moiré Fringes in Strain Analysis*, Pergamon Press, New York, 1969.

[6] Durelli, A. J. and Parks, V. J., *Moiré Analysis of Strain*, Prentice-Hall, Englewood-Cliffs, N.J., 1970.

[7] Post, D. and MacLaughlin, T. F., "Strain Analysis by Moiré Fringe Multiplication," *Proceedings of the Society for Experimental Stress Analysis*, Vol. XXVIII, No. 2, July 1971, pp. 408–413.

[8] Boone, P. and Verbiest, R., "Application of Hologram Interferometry to Plate Deformation and Translation Measurements," *Optica Acta*, Vol. 16, No. 5, 1969, pp. 555–567; also Soete, W., Dechaene, R., and Boone, P., "Toepassingen Van de Holografie, Part A," Research Report, 1970, University of Ghent, Belgium; and Boone, P. M., "Determination of Slope and Strain Contours by Double Exposure Shearing Interferometry," presented at 3rd International Congress Experimental Mechanics, Los Angeles, Calif., May 1973.

[9] Daniel, I. M., Rowlands, R. E., and Post, D., "Moiré Methods for Strain Analysis of Composites," *Experimental Mechanics*, Vol. 13, No. 6, June 1973, pp. 246–252.

[10] Hung, Y. Y. and Taylor, C. E., "Speckle-Shearing Interferometric Camera—A Tool for Measurement of Derivatives of Surface Displacement," *Proceedings, Society Photo-Optical Instrumentation Engineers*, Vol. 41, Aug. 1973, pp. 169–175.

[11] Reinsch, C. H., "Smoothing by Spline Functions," *Numerische Mathematik*, Vol. 10, 1967, pp. 177–183.

[12] Lekhnitskii, S. G., *Anisotropic Plates*, Moscow, 1956, English translation by S. W. Tsai and T. Cheron, Gordon and Breach, New York, 1968.

[13] Powell, R. L. and Stetson, K. A., "Interferometric Vibration Analysis by Wave Front Reconstruction," *Journal of the Optical Society of America*, Vol. 55, No. 12, Dec. 1965, pp. 1593–1598.

[14] Ambartsumyan, S. A., *Theory of Anisotropic Plates*, Technomic Press, Stamford, Conn., 1970.

[15] Aston, J. E. and Whitney, J. M., *Theory of Laminated Plates*, Technomic Press, Stanford, Conn., 1970.